RESEARCH-ARTICLE

Eliminating Channel Feedback in Next-Generation Cellular Networks

DEEPAK VASISHT

SWARUN KUMAR

HARIHARAN SHANKAR RAHUL

DINA KATABI

Published: 22 August 2016

SIGCOMM '16: ACM SIGCOMM 2016 Conference
August 22 - 26, 2016
Florianopolis, Brazil

Conference Sponsors:
SIGCOMM

Eliminating Channel Feedback in Next-Generation Cellular Networks

Deepak Vasisht†, Swarun Kumar‡, Hariharan Rahul†, Dina Katabi†
†MIT CSAIL, ‡ CMU
deepakv@mit.edu, swarun@cmu.edu, rahul@csail.mit.edu, dk@mit.edu

ABSTRACT

This paper focuses on a simple, yet fundamental question: "Can a node infer the wireless channels on one frequency band by observing the channels on a different frequency band?" This question arises in cellular networks, where the uplink and the downlink operate on different frequencies. Addressing this question is critical for the deployment of key 5G solutions such as massive MIMO, multi-user MIMO, and distributed MIMO, which require channel state information.

We introduce R2-F2, a system that enables LTE base stations to infer the downlink channels to a client by observing the uplink channels from that client. By doing so, R2-F2 extends the concept of reciprocity to LTE cellular networks, where downlink and uplink transmissions occur on different frequency bands. It also removes a major hurdle for the deployment of 5G MIMO solutions. We have implemented R2-F2 in software radios and integrated it within the LTE OFDM physical layer. Our results show that the channels computed by R2-F2 deliver accurate MIMO beamforming (to within 0.7 dB of beamforming gains with ground truth channels) while eliminating channel feedback overhead.

1. INTRODUCTION

The high cost of cellular spectrum has motivated network providers to seek advanced MIMO techniques to improve spectral efficiency [22, 3, 54]. Yet, only point-to-point MIMO multiplexing can be performed efficiently in current networks [24]. More advanced MIMO solutions such as massive MIMO [31], coordinated multi-point [32], distributed MIMO [39], and multi-user MIMO [5], all require the base station to know the downlink channels prior to transmission. In the absence of this information, the base station cannot beamform its signal to its users. Today, the only way to learn the downlink channels is to have the user perform the measurements and send the channels back to the basestation. Measuring the channels on the one thousand LTE subcarriers for every antenna on the base station, and feeding those measurements back to the base station generates much overhead [9, 54, 52, 44]. This feedback overhead is excessive even in today's networks which have a limited number of antennas on the base station – about 4.6 Mb/s of signaling per user in a 20 MHz 4×2 network [22, 3]. The problem escalates in future 5G networks which rely on large MIMO systems with many antennas (massive MIMO, CoMP, etc.). In fact, the LTE standardization body that is investigating high-order MIMO systems with up to 64 antennas (Release 13), has declared this problem as a major challenge for future LTE networks [24][1].

SIGCOMM '16, August 22 - 26, 2016, Florianopolis , Brazil

 ISBN 978-1-4503-4193-6/16/08...$15.00
DOI: http://dx.doi.org/10.1145/2934872.2934895

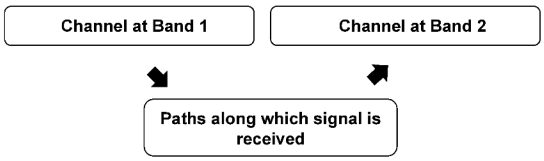

Figure 1: **R2-F2's Approach:** R2-F2 extracts the paths of the signal from channels on band-1 to reconstruct the corresponding channels on band-2.

The goal of this paper is to enable cellular base stations to estimate the downlink channels *without* any user feedback. A natural approach that can help us achieve this goal is channel reciprocity [26]. Reciprocity implies that uplink and downlink channels are the same,[2] so long as both the base station and the clients transmit on the same frequency band. Indeed, reciprocity has been proposed to minimize channel feedback in WiFi networks [33, 15], where both the access point and its clients transmit on the same frequency. Unfortunately, the vast majority of today's cellular connections (including every LTE network in the U.S. [41]) employ Frequency Division Duplexing (FDD) [21], i.e., they transmit data from the phone and base station at different dedicated frequency bands. Thus, extending reciprocity to LTE networks requires answering the following fundamental question: *How do we infer the wireless channels on one frequency band by observing those channels on a different band?*

[1]For example, with 64-antenna base stations, the need to learn the downlink channels consumes 48% of the traffic generated by the base station, simply to send per-antenna reference signals [24].

[2]Modulo a constant factor.

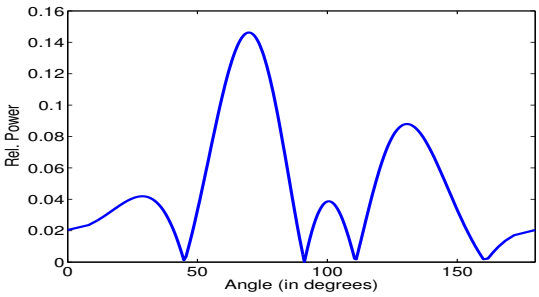

Figure 2: **Power Profile:** The power profile represents the relative power of the signal coming along different spatial directions.

We introduce R2-F2, a system that does exactly that – i.e., it can infer the RF channels on one band by observing them on a different band. Before we dive into R2-F2, let's explain why wireless channels vary across frequency bands in the first place. RF signals are waves whose phase changes with time and frequency. The wireless channels are the result of those waves traversing multiple paths, reflecting off walls and obstacles, then combining at the receiver. Due to their frequency-dependent phases, RF waves that combine to reinforce each other on one frequency may cancel each other on another frequency. As a result, wireless channels could look quite different at different frequencies.

R2-F2 infers wireless channels across frequencies by leveraging a simple observation: while the channels change with frequencies, the underlying physical paths traversed by the signal stay the same. Hence, R2-F2 operates by identifying a transform that allows it to map the observed channels to the underlying paths, then map them back to the channels at a different frequency, as shown in Fig. 1.

But how do we identify a frequency-invariant transform for mapping channels to paths? It is natural to look into past work on RF-based localization systems since, like us, they need to relate RF channels to the underlying paths. Localization systems [53, 27, 4, 29, 28] exploit the MIMO antennas on a base station to create a power profile that shows the spatial directions of the incoming signal, as illustrated in Fig. 2. Each peak in the profile is, then, associated with the direction of an underlying path. Unfortunately, these localization power profiles are unsuitable for our purpose. While they reveal information about the direction of the signal, they lack information about the exact distance travelled by the signal and whether the path is direct or reflected off a wall. Such missing parameters introduce frequency-dependent phase variations in RF waves travelling along different spatial paths, and hence, change the channel values. Furthermore, in §4, we show that, due to windowing and superposition effects, the power profiles change with frequency and deviate from the spatial directions of the underlying paths. Our empirical results in §8 demonstrate that using the localization power profiles for recovering the underlying channels eliminates 60% of MIMO SNR gains.

R2-F2 builds on the insights learned from RF-localization, but it is the first to enable LTE base stations to infer the downlink channels without any feedback, and at an accuracy suitable for MIMO techniques. In §5, we explain how we design a channel-to-path transform that incorporates the information needed to predict channels across frequencies. We further embed this transform in a full system that overcomes additional practical challenges, including accounting for: (1) frequency offset between the user and the base station; (2) hardware differences in transmit and receive chains; and (3) packet detection delay — all of which affect wireless channels differently at different frequency bands.

We built R2-F2 in USRP radios and integrated it with LTE OFDM. Our testbed emulates a small cell setting with a 5-antenna LTE base station. We deploy our base station within a few meters from one of the LTE base stations on our campus. Since we cannot transmit in the cellular spectrum, we operate our testbed on the 640-690 MHz white space frequency band, which is in the vicinity of the Verizon LTE band (only 30 MHz away). Our results reveal the following:

- For an uplink-downlink frequency separation equal to that in AT&T and Verizon networks, the channels computed by R2-F2 deliver accurate MIMO beamforming within 0.7 dB of the beamforming obtained with the ground-truth channels. The resulting SNR increase has improved the average data rates in our testbed by 1.7×. This result shows that R2-F2 can be used by MIMO solutions to deliver LTE throughput gain while eliminating channel feedback overhead.
- R2-F2 can also be used to eliminate interference at cell edges and improve spatial reuse. In our testbed, R2-F2 reduced the SNR of the interfering signal from 9 dB to only 0.9 dB.
- The quality of R2-F2's inferred channels remains high across frequencies separated by up to 40 MHz, which is larger than the LTE uplink-downlink separation in most US LTE deployments. Further, the degradation of SNR with uplink-downlink separation is less than 0.2 dB per 10MHz.

To our knowledge, R2-F2 is the first system that demonstrates the practicality of inferring LTE downlink channels from uplink channels using reciprocity and without channel feedback. This result contributes a better understanding of reciprocity in FDD systems, and a solution to one of the important challenges facing future 5G MIMO networks.

2. Related Work

Related work falls under two broad categories.

(a) Channel Estimation in Cellular Networks: Much prior work has reported the excessive overhead associated with channel estimation and feedback in cellular networks [9, 54, 22, 52, 44]. Even in today's networks, which have a relatively small number of antennas, the feedback overhead can be prohibitive – as much as 4.6 Mb/s of signalling traffic per user in a 4×2 system [22, 3]. All recent LTE releases recognize this challenge [3, 2, 1]. To mitigate the problem, the standard allows for either sending full channel information, or compressing the information using a codebook of limited values. Unfortunately, neither option is satisfactory since the former causes excessive overhead,

whereas the latter leads to poor channel resolution that impedes the gains of MIMO techniques [34, 14, 25]. As a result, only point-to-point MIMO is common in today's LTE networks (in the US), and more advanced techniques, such as MU-MIMO have yet to gain deployment traction [13]. This problem is increasingly critical with the advent of 5G networks which rely on large MIMO systems (e.g., massive MIMO) to increase spectral efficiency [30, 45].

Past work on addressing this problem has focused on various techniques for compressing channel feedback [9, 54, 40, 45]. R2-F2 is motivated by the same desire of learning downlink channels with minimal overhead, but it aims to eliminate channel feedback altogether, and replace it with passive inference of channel values.

A few papers study reciprocity in the context of FDD systems. In particular, Hugl et. al [19] observe that the channels at two cellular FDD bands are correlated and hence postulate that one can infer downlink channels from uplink channels. Some papers [18, 20, 36, 37] propose theoretical models that use large antenna arrays to infer channels on the downlink from those on the uplink. Their models are either based on long-term channel statistics and do not account for fast variations, or are based on the angle of arrival power profile (used in RF localization), which we show in §8 to yield poor performance in practice. Further, they do not account for practical challenges in system design such as the limited LTE bandwidth (typically 10MHz), carrier frequency offset (CFO) and detection delay. In contrast, R2-F2 does not need long-term statistics and is empirically demonstrated in a testbed deployment. R2-F2 achieves this through a new design that relates the channels to frequency-invariant parameters (e.g., path lengths), compensates for frequency dependent parameters (e.g., path phases), and accounts for distortion factors (e.g., window effect).

(b) Related Work Outside Cellular Networks: R2-F2 is related to the problem of channel quality estimation. Some applications aim to infer channel quality on a particular frequency band, but do not need the exact channel values. For example, two WiFi nodes may want to select the best quality WiFi channel for their connection without actively running measurements on all WiFi channels [10, 42]. The same applies to cognitive radios in the White Spaces [38]. These systems observe the channel on one or more bands and use that information to infer the SNR of the channel on a different band –i.e., the channel quality. In contrast, R2-F2 needs to infer the full channel values–i.e., it needs both the phase and the magnitude of the channel for every OFDM sub-carrier and every antenna.

R2-F2 is also related to past work that focuses on estimating the channels across a large band of spectrum by subsampling the frequencies in that band. For example, the work in [6] subsamples the spectrum and uses compressive sensing to recover the channel values at the missed bands. This approach does not apply to LTE networks since the observed uplink channels do not satisfy the sampling requirements of compressive sensing (i.e. the uplink channel is only available on one contiguous band).

There is also a large body of work that aims to predict wireless channels in the future based on their values in the past [51, 8, 12]. This work does not predict channels across frequency bands. R2-F2 is complementary to this work in that it estimates wireless channels at different values of frequency as opposed to different points in time.

Finally, we note that R2-F2 is related to a wide range of systems for the TV whitespaces that aim to predict occupancy [7, 43] or interference [55] by hopping between a minimal number of frequency bands. R2-F2 complements these systems by estimating the wireless channel at any target frequency band based on sampling the channel at one other band.

3. BACKGROUND

In this section, we list a few known results in modeling wireless channels, which are important for the rest of the exposition. Note that the mathematical expressions refer to the transmission frequency by the corresponding wavelength λ.

Wireless channels describe how the signal changes as it propagates from transmitter to receiver. They are a direct function of the paths along which the signal propagates as well as the transmission frequency. In particular, the channel of a narrowband signal traversing a single path is given by [47]:

$$h = ae^{-j2\pi\frac{d}{\lambda}+j\phi} \tag{1}$$

where λ is the wavelength, a is the path attenuation, d is the distance the path traverses, and ϕ is a frequency-independent phase that captures whether the path is direct or reflected.

Since the signal travels along multiple paths, say N, the channel at a receive antenna can be written as:

$$h = \sum_{n}^{N} a_n e^{-j2\pi\frac{d_n}{\lambda}+j\phi_n}, \tag{2}$$

which is the sum of the channel components over all paths that the signal takes between transmitter and receiver.

Finally, we note that base-stations have multiple antennas, so they obtain one channel per antenna. For a K antenna base station, the set of channels, h_i on antenna i is:

$$h_i = \sum_{n}^{N} \left(a_n e^{-j2\pi\frac{d_n}{\lambda}+j\phi_n}\right) e^{-j2\pi\frac{il\cos\theta_n}{\lambda}}, \tag{3}$$

where θ_n is the angle-of-arrival of the signal along path n, d_n is the distance travelled by the signal along path n to the first antenna and l is the pairwise separation between antennas on the base station. Note that the above equation depends both on frequency and all underlying signal propagation paths.

4. INTUITION UNDERLYING R2-F2

R2-F2's primary objective is to infer wireless channels on a target frequency band, given the wireless channels on a different frequency band. In order to achieve this objective, R2-F2 relies on the observation that the channels are the direct result of the signal paths. While the channels change

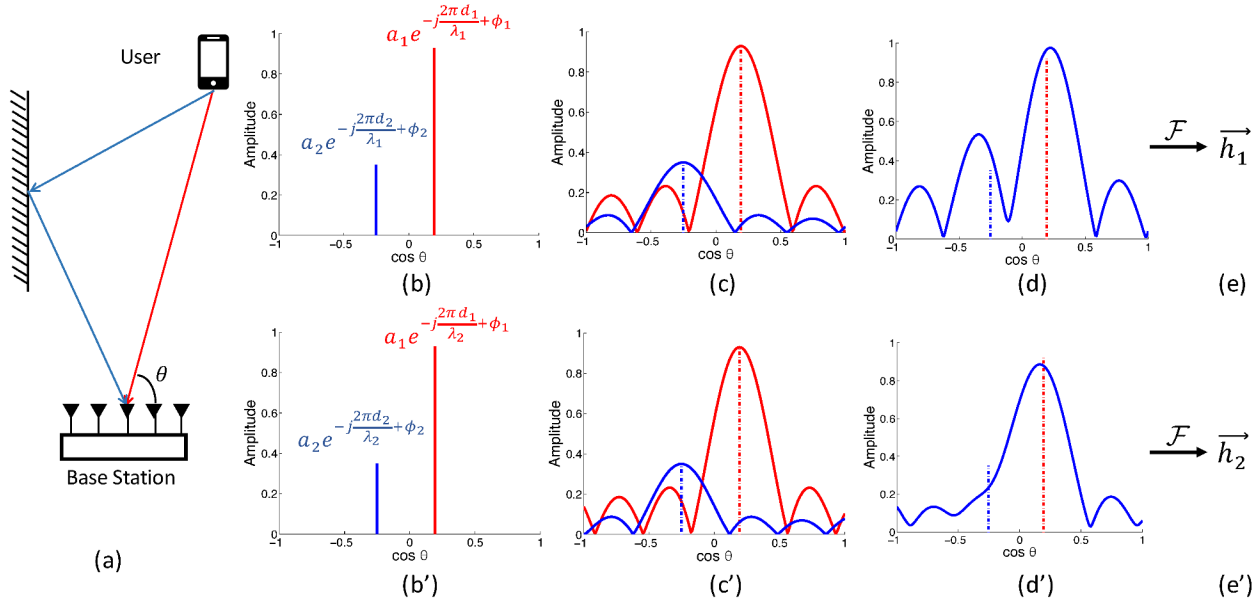

Figure 3: **Transforming Signal Paths to Channels on Two Frequency Bands:** (a) Consider two signal paths emerging from 80° and 105° as shown. Their corresponding attenuations are: a_1, a_2, distances traversed are d_1, d_2, and phase offsets due to reflectors (or lack there-of) ϕ_1, ϕ_2. (b)-(b') Depicts the signal components of individual paths across angle-of-arrival. We observe two spikes at 80° and 105° as expected scaled by the respective path amplitudes. The peaks differ only in phase. (c)-(c') Incorporates the windowing effect that causes the peaks to be convolved with sinc functions. The red and blue sinc correspond to the red and blue path. Further, the width of the sincs changes with frequency. (d)-(d') Depicts the superposition of the sinc functions in both frequency bands. The two plots look very different – both due to the difference in shape of the sincs as well as the difference in their phases. (e)-(e') Denotes the wireless channels obtained after applying the Fourier Transform on the two bands – two different sets of values.

across frequencies, the underlying paths stay the same. Thus, if one could obtain a frequency-invariant representation of signal paths from wireless channels on any given frequency, one can recreate an estimate of the channels at any other frequency of interest.

But what is a frequency-independent representation of signal paths that can be mapped to (and from) wireless channels? The answer to this question lies in Eqn. 3, which defines wireless channels based on underlying propagation paths. Specifically, wireless channels h_i depend on four distinct attributes of signal paths: (1) Their attenuation a_n; (2) Their frequency-independent phase ϕ_n, that distinguishes the direct path from reflected paths; (3) Their angle of arrival θ_n; (4) The distance they traverse d_n. These four quantities, when listed for each path, fully define the wireless channels on any given frequency. More importantly, none of these parameters depend on the frequency at which the channel is obtained. In other words set of four-tuples of the form $(a_n, \phi_n, \theta_n, d_n)$ is a natural representation of signal paths that is frequency-invariant.

Now that we have a representation of signal paths, we need to understand how to extract it given wireless channels on any frequency. To do so, observe that wireless channels in Eqn. 3 take the form of the familiar discrete Fourier transform (parameterized by spatial angle-of-arrival $\cos\theta$). In particular, this Fourier transform takes as input quantities that depend directly on our signal path four-tuples. Since the discrete Fourier transform is invertible, one might wonder if we can simply apply the inverse Fourier transform to retrieve the signal paths given wireless channels. Unfortunately, our task is not this simple. This is because, upon inverting the Fourier transform, we get quantities that depend not just on our signal path four-tuples, but also the frequency. As a result, teasing apart signal four-tuples from wireless channels requires removing this dependency on frequency.

To understand how to achieve this, it is instructive to study how the same signal 4-tuples manifest as different wireless channels on two different frequencies, say 600MHz and 650MHz. We do so in the context of a specific example. Consider Fig. 3(a) which depicts signals from the phone to the base station traversing two paths. Let the corresponding signal path 4-tuples be: $(a_1, \phi_1, \theta_1 = 80^o, d_1 = 19.5m)$ and $(a_2, \phi_2, \theta_2 = 105^o, d_2 = 23m)$. These undergo four distinct transformations, inclusive of the Fourier transform, before they become the overall wireless channels on the two frequencies (from Fig. 3(a) to (e)-(e')) as described below:

- **Phase Variation (Fig. 3(a) to (b)-(b')):** We first begin by mapping the signal path 4-tuples to inputs of the Fourier tranform. Recall from Eqn. 3 that these inputs are simply the wireless channel components along individual paths at the two frequencies. Fig. 3(b)-(b') visualizes the amplitude and phase of the signal components from the two paths across angle-of-arrival. As expected, both these plots have two spikes that correspond to the two paths, scaled by their respective attenuations. In fact, the two

plots differ only in the phase of the spikes, which scales inversely with the wavelength of the two bands.

- **Windowing Effect (Fig. 3(b)-(b') to (c)-(c')):** Before we can apply the Fourier transform, we need to account for an effect that occurs since the cellular base station has a limited number of antennas (5 in our example). Specifically, this means that the base station samples the signal from the two paths within a window of space (the space between the first and last antenna). Since the channels are observed only within a window of space, the signal's angles of arrival are convolved with a sinc function. This is a standard property of the Fourier transform: multiplying by a window in one domain translates into a convolution with a sinc in the other domain. Thus each impulse from the corresponding angle as in Fig. 3(b) and (b') is transformed as a sinc function as shown in Fig. 3(c) and (c'). The convolution with a sinc makes the signal look different across frequencies. Specifically, the precise shape of the sinc changes with the transmission frequency. This is because the distances between antennas are measured relevant to the wavelength of the transmission signal. Hence, at higher frequency the distance between antennas seem larger and the sinc narrower.
- **Superposition (Fig. 3(c)-(c') to (d)-(d')):** At this point, the signals components from different paths super-impose at the receiver. Thus, the base station gets a super-position of the blue and red sincs in Fig. 3(b) and (b'), scaled by their respective phases that (as described earlier) are different. This results in Fig. 3(d) and (d') that now look significantly different.
- **Fourier Transform (Fig. 3(d)-(d') to (e)-(e')):** Finally, we apply the Fourier transform to take our super-imposed sincs in Fig. 3(d) and (d') to the wireless channels sampled at the five antenna locations, and shown in Fig. 3(e) and (e').

Thus, if we want to move from wireless channels to their underlying signal paths, we must invert this whole process. We need to: (1) Invert the Fourier transform; (2) Separate the super-imposed sincs; and (3) Undo the windowing effect; (4) Correct for the difference in phase between the two frequencies. In the next section, we describe this process mathematically and formulate it as an L-2 minimization problem.

5. ALGORITHM

In this section, we formalize the discussion in §4. We begin by formalizing mathematically the transform between wireless channels and signal paths. We then invert the effects of this transform by formulating the problem as an L-2 optimization whose solution results in the frequency-invariant signal path characteristics. These paths are then used to infer the channels on a desired band.

5.1 Transforming Physical Paths to Wireless Channels

Let us assume that the signal from the user to the K-antenna base station arrives along N distinct paths. The antennas are indexed by $0, 1, \ldots, K-1$ and l is the inter-antenna separation.[3] Further, let us denote the signal path 4-tuple of the n^{th} path to be $(a_n, \phi_n, \theta_n, d_n)$. The setup (with just one path) is illustrated in Fig. 4.

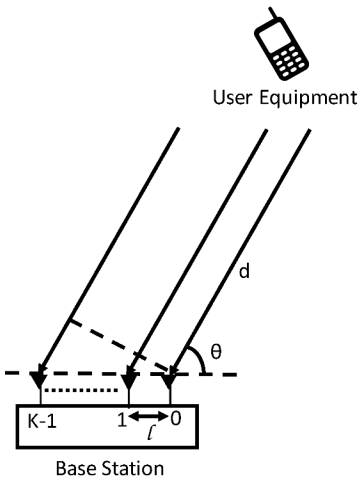

Figure 4: **Antenna Setup** The base station is equipped with multiple antennas and receives signals on a fixed bandwidth.

We now present the mathematical formulations of the individual transforms described in §4, between our signal path representation and wireless channels (see Fig. 3).

- **Phase Variation:** Since the Fourier transform described in equation 3 operates on the $\cos\theta$ domain, we discuss the algorithm in terms of $\cos\theta$. Let us denote $\psi = \cos\theta$. Then, the contribution of the n^{th} path to the directional representation of the signal at wavelength, λ_1 can be given by:

$$P_1^n(\psi) = a_n e^{-j\frac{2\pi d_n}{\lambda_1} + j\phi_n}\delta(\psi - \psi_n), \tag{4}$$

  where $P_1^n(\psi)$ represents the signal component along direction ψ and $\delta(.)$ is the impulse function. ϕ_n denotes the phase accumulated by the n^{th} path by virtue of undergoing reflections, a_n is the amplitude of the path as received on antenna 0 and $\psi_n = \cos\theta_n$. This representation corresponds to the representation in Figs. 3(b) and (b').
- **Windowing Effect:** As described before, the signal sensed by the antenna array along different spatial directions is the inverse Fourier transform of the channel measurements on the different antennas of the antenna array. Since the antennas on the base station sample a finite space, it is equivalent to applying a window on the antenna domain of width $\frac{L}{\lambda_1}$, where L $(= Kl)$ is the width of the antenna array. This creates a *sinc* in the spatial direction domain, i.e. the path directions get convolved with $\frac{L}{\lambda_1} sinc\left(\frac{L\psi}{\lambda_1}\right)$. Thus, if we represent the spatial profile after

[3] In typical antenna arrays, the inter-antenna spacing is set to $\frac{\lambda}{2}$, where λ is the signal wavelength.

convolution of the sincs with P_1^n as P_2^n, then P_2^n is given by

$$P_2^n(\psi) = \{a_n e^{-j\frac{2\pi d_n}{\lambda_1}+j\phi_n}\delta(\psi-\psi_n)\} * \frac{L}{\lambda_1} sinc\left(\frac{L\psi}{\lambda_1}\right) \tag{5}$$

where $*$ denotes convolution operation. Thus, $P_2^n(\psi)$ refers to the graphs in Figs. 3(c) and (c').

- **Superposition:** In case of multiple paths, the perceived path profile is simply the sum of individual path profiles. Thus, the overall profile $P_3(\psi)$, can be computed as:

$$P_3(\psi) = \sum_{n=0}^{N-1} P_2^n(\psi). \tag{6}$$

This equation mathematically represents Fig. 3(d)-(d').

- **Discrete Fourier Transform:** Finally, the channel measurements at the antennas are just the Fourier transform of the signal arriving along spatial directions. In order to represent this mathematically, observe that equation 6 can be simplified as follows:

$$P_3(\psi) = \sum_{n=0}^{N-1}\{a_n e^{-j\frac{2\pi d_n}{\lambda_1}+j\phi_n}\delta(\psi-\psi_n)\} * \frac{L}{\lambda_1} sinc\left(\frac{L\psi}{\lambda_1}\right) \tag{7}$$

$$= \sum_{n=0}^{N-1} a_n e^{-j\frac{2\pi d_n}{\lambda_1}+j\phi_n} \times \frac{L}{\lambda_1} sinc\left(\frac{L(\psi-\psi_n)}{\lambda_1}\right) \tag{8}$$

Equation 7 follows from equation 8 by using the convolution property of the delta function.

The above four transformations can be summarized succinctly as a sequence of matrix operations. Specifically, given that the antennas are positioned at K discrete locations in space, we can now represent the Fourier transform by a matrix multiplication. Let us define $\mathbf{F}$ to be the $K \times K$ Fourier matrix, such that $\mathbf{F}_{ij'} = e^{-j\frac{2\pi i j' \psi'}{\lambda_1}}$, where ψ' defines the discretization on the variable ψ ($\psi' = \frac{2}{K}$).[4] Further, define $\mathbf{S}$ to be the $K \times N$ matrix where $\mathbf{S}_{ij}$ denote the value of the sinc function corresponding to the j^{th} path at $\psi = i\psi'$. Specifically, $\mathbf{S}_{ij} = \frac{L}{\lambda_1} sinc\left(\frac{L(i\psi'-\psi_j)}{\lambda_1}\right)$. Finally, define $\vec{a}'_1$ to be the N dimensional vector such that the i^{th} component is $a_i e^{-j\frac{2\pi d_i}{\lambda_1}+j\phi_i}$. Then, the channel measurements at the antennas, represented by $\vec{h}_1$ can be given by:

$$\vec{h}_1 = \mathbf{F}\mathbf{S}\vec{a}'_1 \tag{9}$$

Note that, $\vec{h}_1$ is the K dimensional vector such that the k^{th} element represents the channel measurement at antenna k. Observe that, in the vector notation, the i^{th} component of $\mathbf{S}\vec{a}'_1$ is nothing but $P_3(i\psi')$. In summary, we now have a transform that maps signal paths to channels.

[4]When the antenna separation, l, is not equal to $\frac{\lambda_1}{2}$, the Fourier matrix is replaced by the non-uniform Fourier matrix and $\psi' = \frac{\lambda}{L}$, where $L = Kl$ is the total antenna array aperture.

5.2 From Wireless Channels to Paths

Now that we understand, how the channels are derived from the underlying physical paths, the goal is to find a way to invert this mechanism. In other words, given channel measurements, $\vec{h}_1$ on wavelength λ_1, we need to identify the underlying physical paths. We do so by inverting the individual components of the transform – the Fourier Transform, windowing and super-position and phase variations.

Inverting the Fourier Transform: The first step is to invert the effect of the Fourier transform, which is simply the inverse Fourier transform on the channel measurements, $\vec{h}_1$. This can be achieved by multiplying $\vec{h}_1$ by $\mathbf{F}^{-1}$.

Inverting Windowing and Superposition: Next, we need to invert the superposition effect, stated in equation 6 and the windowing effect from equation 5. These two effects are jointly represented by the matrix multiplication, $\mathbf{S}\vec{a}'_1$ in equation 9. The goal is to infer $\mathbf{S}$ and $\vec{a}'_1$, given the perceived signal paths, $\mathbf{F}^{-1}\vec{h}_1$. Observe that, $\mathbf{S}$ depends solely on the directions of the underlying paths (ψ_n). Thus, in order to compute $\mathbf{S}$, we need to find $\{\psi_n\}_{n=0}^{N-1}$ for each of the N sinc functions that sum up to yield this profile. We pose this problem as an L-2 norm minimization problem. We optimize for $\{a'_{1,n}\}_{n=0}^{N-1}$ and $\{\psi_n\}_{n=0}^{N-1}$ such that $||\mathbf{F}^{-1}\vec{h}_1 - \mathbf{S}\vec{a}'_1||^2$ is minimized. Let us write this objective function as:

$$O(\{a'_{1,n}, \psi_n\}_{n=0}^{N-1}) = ||\mathbf{F}^{-1}\vec{h}_1 - \mathbf{S}\vec{a}'_1||^2 \tag{10}$$

where $a'_{1,n}$ denotes the n^{th} element of $\vec{a}'_1$

In order to simplify the problem, observe that, if we know $\mathbf{S}$, the optimization problem becomes a linear optimization problem and can be solved for $\vec{a}'_1$ in the closed form. In particular, the minimum value can be attained by setting $\vec{a}'_1 = \mathbf{S}^\dagger\mathbf{F}^{-1}\vec{h}_1$, where $\mathbf{S}^\dagger$ denotes the pseudo-inverse of $\mathbf{S}$.

Thus, the objective function in equation 10 can be reframed as:

$$O(\{\psi_n\}_{n=0}^{N-1}) = ||\mathbf{F}^{-1}\vec{h}_1 - \mathbf{S}\mathbf{S}^\dagger\mathbf{F}^{-1}\vec{h}_1||^2 \tag{11}$$

We have, now, reduced the problem to identifying the directions of the signal paths that contribute to the directional signal profile. This objective function, however, is non-linear and non-convex. We discuss in §5.3 how we find a solution to this optimization problem.

Accounting for Phase Variation: Finally, in order to infer channels at a different wavelength, λ', we need to fit in another missing piece. Recall that the phase of $a'_{1,n}$ inferred at wavelength, λ_1 for each of the paths, is dependent on the wavelength (since $a'_{1,n} = a_n e^{-j\frac{2\pi d_n}{\lambda_1}+j\phi_n}$). In order to infer the frequency-dependent component of $a'_{1,n}$, we leverage the fact that for cellular systems, the wireless signal is transmitted at multiple frequencies, called the OFDM subcarriers. This gives us access to channel measurements on multiple frequencies. Thus, we add the distance d_n for each of the paths as a parameter of the optimization problem given in equation 10. This allows us to solve the optimization problem jointly for multiple subcarriers and adds constraints to the solutions returned by the optimization at different frequencies.

In particular, let us denote the channel measurements at wavelength, λ_i, by $\vec{h}_i$, $i = 0, 1, \ldots, I-1$. We define $\vec{P}_i = \mathbf{F}^{-1}\vec{h}_i$, and $\mathbf{S}_i$ to be the matrix $\mathbf{S}$ corresponding to wavelength λ_i. Let, $\mathbf{D}_i$ be the $N \times N$ diagonal matrix such that $\mathbf{D}_i(k,k) = e^{-j\frac{2\pi d_k}{\lambda_i}}$ and $\vec{a}$ be the N dimensional vector such that i^{th} element is $a_i e^{j\phi_i}$. Let $\vec{\mathcal{P}}$ denote the IK dimensional vector formed by the concatenation of the vectors $\vec{P}_i$ and $\mathbf{S}$ be the $IK \times N$ matrix formed by the concatenation of the matrices $\mathbf{S}_i\mathbf{D}_i$. Specifically:

$$\vec{\mathcal{P}} = \begin{pmatrix} \vec{P}_1 \\ \vec{P}_2 \\ . \\ . \\ \vec{P}_K \end{pmatrix} \quad \mathcal{S} = \begin{pmatrix} \mathbf{S}_1\mathbf{D}_1 \\ \mathbf{S}_2\mathbf{D}_2 \\ . \\ . \\ \mathbf{S}_K\mathbf{D}_K \end{pmatrix} \tag{12}$$

Thus, the modified objective function can be written as:

$$O(\{\psi_n, d_n, a_n\}_{n=0}^{N-1}) = ||\vec{\mathcal{P}} - \mathcal{S}\vec{a}||^2 \tag{13}$$

This objective function is similar to equation 10. Like before, we can replace $\vec{a} = \mathcal{S}^\dagger\vec{\mathcal{P}}$. Thus, the objective function reduces to:

$$O(\{\psi_n, d_n\}_{n=0}^{N-1}) = ||\vec{\mathcal{P}} - \mathcal{S}\mathcal{S}^\dagger\vec{\mathcal{P}}||^2 \tag{14}$$

5.3 Solving the Optimization

In this section, we describe how we solve the optimization problem that transforms channels to paths. Our goal is to find the values of $\{\psi_n, d_n\}_{n=0}^{N-1}$, such that:

$$\begin{aligned} &\{\psi_n, d_n\}_{n=0}^{N-1} = \arg\min_{\psi_n, d_n} O(\{\psi_n, d_n\}_{n=0}^{N-1}) \\ &\text{s.t.} \quad -1 \leq \psi_n \leq 1 \quad \forall n \in \{0, 1, \ldots, N-1\} \end{aligned} \tag{15}$$

This optimization problem is non-convex and constrained. In order to solve this optimization problem, we use the well-known interior-point method. However, since the function is non-convex, the optimization is prone to convergence to a local minimum, which is not the global minimum. Thus, a good initialization is important to ensure that the correct solution is determined.

- **Initialization:** R2-F2 computes an approximate solution in order to initialize the minimization of the objective function described in equation 14. We compute an approximate probability distribution, P such that $P(d, \psi)$ indicates the probability of the existence of a path from direction ψ and distance d. A natural candidate to do so is the power of the inverse Fourier transform of the channel itself (akin to Fig. 3(c)-(c')), which while prone to the windowing and superposition effects provides an approximate understanding of where signal paths emerge from. Generalizing the inverse Fourier transform to operate across both distance and angle-of-arrival, we define P to be:

$$P(d, \psi) = || \sum_{i=1,\ldots,I; k=1,\ldots,K} h_{i,k} e^{j\frac{2\pi(d + kl\psi)}{\lambda_i}} ||^2$$

  where $h_{i,k}$ denotes the channel measured at antenna k and wavelength λ_i and l is the inter-antenna separation on the antenna array. Once, P has been computed for different values of d and θ, we pick the N largest peaks to initialize the optimization problem with N paths.
- **Stopping Criterion:** So far, we have assumed that we know the number of paths, N, a priori. However, that is not the case in practice. Notice that, as we increase the number of paths, N, in our objective function, the minimum value attained on the objective function decreases. In other words, the algorithm keeps finding a better fit. However, after certain number of paths, we start to overfit, i.e., the additional paths being found do not correspond to physical paths, but to signal noise. This could lead to decrease in the accuracy of our channel estimation algorithm. In order to avoid overfitting and yet achieve a good fit, we incrementally add paths to the solution till one of the two conditions is met. Either, the value of the objective function drops below a threshold,ϵ[5] or decrease in the value of the objective function is small. When that happens, we select that value of N as the number of paths.
- **Conditioning:** When the number of paths, N, is greater than 1, the optimization can find solutions, such that (ψ_i, d_i) is very close to (ψ_j, d_j) for $i \neq j$, i.e. two paths come from nearly the same angle and distance. In that case, the matrix $\mathcal{S}$ becomes ill-conditioned and can lead to poor solutions. In such cases, R2-F2 rejects one of these paths and reduces the number of paths by 1. This improves the condition number of the matrix and avoids overfitting.

6. INTEGRATING R2-F2 WITH THE LTE ARCHITECTURE

This section describes R2-F2's end-to-end system design, and how it interacts with the LTE protocol. R2-F2 takes as inputs wireless channels measured on the uplink at the base station for a particular user. It outputs the estimated wireless channels at the downlink frequency band for that user. These channels can then be used to perform beam-steering for advanced MIMO techniques (coherent beamforming, interference nulling, etc.).

The following steps summarize R2-F2's approach: (1) R2-F2 runs an iterative algorithm to find a representation of signal paths that fit the observed uplink channels. This is done by solving the optimization in Eqn. 14 as described in §5.3. (2) R2-F2 use the recovered 4-tuple signal paths to map the uplink channels to the frequency used on the downlink channel (Eqn. 9). (3) Now that it has the values of the uplink channels for the downlink frequency, R2-F2 applies standard reciprocity [16] to infer the downlink channels.[6] Fig. 5 presents an overview of R2-F2's architecture.

We next discuss a couple of issues that arise when integrating the above steps with LTE cellular systems.

6.1 Measuring the Uplink Channels

[5]We set ϵ to $0.01 \times IK$, where IK is the number of elements in h.

[6]Standard reciprocity infers the forward channels from the reverse channels by multiplying by calibrated reciprocity constants, which are computed once for the lifetime of the device as described in [16].

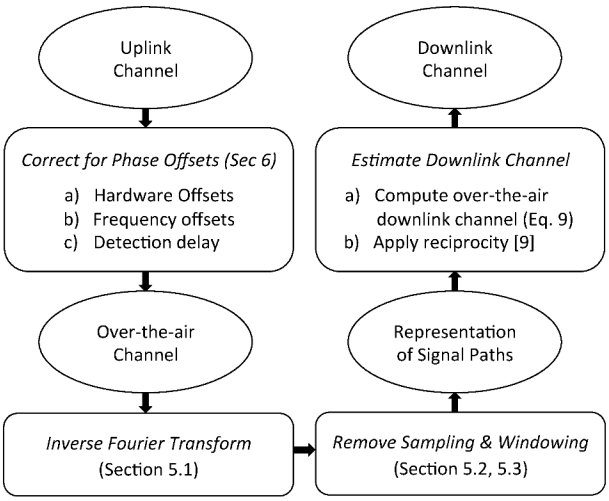

Figure 5: **R2-F2's System Design:** The above diagram summarizes the steps in R2-F2's system design in translating channels at the base station measured on the uplink to channels at the user on the downlink frequency bands.

In R2-F2, the base station measures the uplink channels in order to infer the downlink channels. However, since LTE uses SC-FDMA on the uplink, the client transmits its data only on a subset of all OFDM subcarriers. Thus, while LTE uses one thousand subcarriers, only a subset of those subcarriers can be used to measure the uplink channels for a particular client at any point in time. However, in LTE, a client does not only send data. It also sends signaling information. In particular, the LTE standard uses Sounding Reference Signals (SRS) [3] which the client sends periodically across OFDM subcarriers. The period of the SRS signal is configurable and takes values between 2ms and 320ms. Thus, R2-F2 measures the uplink channels using the SRS transmissions. It further refines these channels with measurements from uplink data and acknowledgments, which can provide new measurements every 1 ms, but span only a subset of the OFDM sub-carriers. Combining all these measurements allows R2-F2 to obtain a better estimate of the uplink channels, which naturally improves its inference of the downlink channels.

One however has to be careful when combining channel measurements that did not occur at exactly the same time. Measurements taken at different times can be affected by the carrier frequency offset (CFO) between the transmitter and receiver, frame detection delay as well as inherent delays in hardware. We discuss these effects and how we compensate for them before combining the channel measurements.

- **Frequency Offset:** Between any client and the base station, there always exists an offset in frequency (CFO), δf. The CFO causes a phase rotation over time. Thus, two measurements of the same channel that are taken τ seconds apart, exhibit a phase difference of $2\pi\tau\delta f$. This phase difference is a measurement artifact; the channels over the air have not changed. To overcome this issue, we leverage the fact that for all MIMO techniques (beamforming, nulling, interference alignment, etc.) the parameter of importance is not the exact value of the wireless channels, but the relative change in the channels across the antennas. As a result, a constant multiplied to the channel measurements on all antennas does not affect our ability to perform all MIMO techniques. Thus, since all antennas on the base station experience the same CFO, we can eliminate the phase rotation caused by CFO by dividing the channel of each base station antenna by the channel of the first antenna, measured at the same point in time. This division scales all channels by the same value and hence does not affect MIMO techniques.
- **Frame Detection Delay:** There is a time delay between the moment the signal reaches the radio and the moment when it actually gets detected. This delay causes an additional phase rotation in the measured channels. If we denote this detection delay by t_d, the additional phase rotation is given by $2\pi f t_d$. The channel measurements on all the antennas get effected by this quantity. This detection delay varies per measurement and thus, makes it infeasible to combine information across different measurements without eliminating the phase rotation due to the detection delay. To overcome this challenge, observe that across OFDM subcarriers any delay in time manifests itself as rotation in phase across subcarrier frequency whose slope is exactly $2\pi t_d$. As a result, R2-F2 can enforce consistency between measurements of the wireless channel at any given frequency by ensuring they have zero relative slope in phase.
- **Hardware Delay:** The hardware across different antennas introduces a fixed delay to the different receive chains. Thus, the wireless channel measured at each antenna suffers a phase rotation. In particular, the channel measured at an antenna with hardware delay t experiences an additional offset $e^{-j\frac{2\pi ct}{\lambda}}$, where λ is the wavelength of the signal and c is the speed of light. Further, this offset is different for different receive chains. Fortunately, hardware-induced phase offset is fixed for the lifetime of the base station and can be calibrated once, apriori and applied to all future channel measurements.

6.2 Inter-cell Interference

R2-F2's channel estimates can be used to improve overall throughput by reducing inter-cell interference at edge clients – devices that are close to cell boundaries and hence, receive signal from multiple base stations. R2-F2 adopts two strategies to limit the interference caused at edge clients by neighboring base stations: (1) It encourages sharing of information between adjacent base stations to predict uplink channels to users across base stations. This allows the base station to estimate the client channels and learn any potential interference from the channel estimates of its neighboring base stations. (2) Base stations can use the channel estimates they infer from R2-F2 to transmit to their clients while nulling interference to clients of other base stations that happen to be at cell edges. Indeed, the same wireless channels used for beamforming can be employed for interference nulling as well. Our results in §8 show that interference nulling at

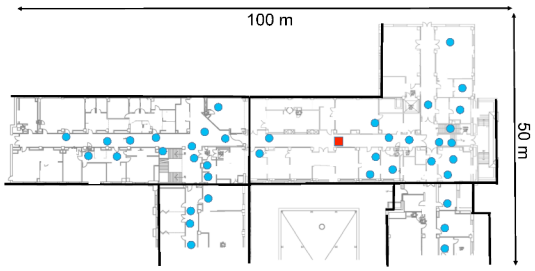

(a)

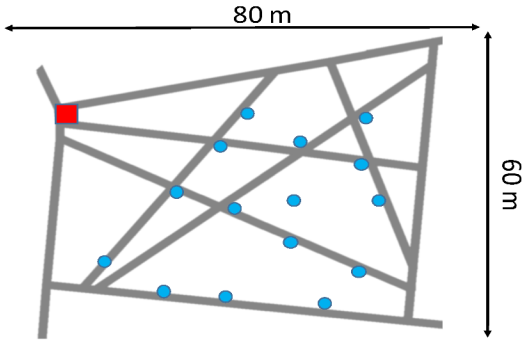

(b)

Figure 6: **Experiment Testbed:** (a) plots the indoor testbed for our experiments. Thick black lines indicate building boundaries. The floor map of individual buildings is marked inside each building. Experiments were conducted in the publicly accessible spaces across four buildings. (b) is the outdoor testbed with roads and pathways shown; buildings have been removed for anonymity. In (a) and (b), the red square marks the presence of the base station and the blue dots represent the clients.

edge clients using R2-F2 leads to improved throughput in LTE networks.

7. Implementation

We implemented R2-F2 on a five-antenna Ettus USRP N210 software radio platform emulating a five-antenna LTE base station. The USRPs are synchronized using an external clock and act as a five-antenna MIMO node. They transmit using an OFDMA architecture that transmits 1024 subcarriers over 10 MHz, which are parameters identical to common LTE deployments of major US operators [3]. We implement LTE's OFDMA by modifying the Ettus UHD driver for USRP software radios. Our software radios operate over the whitespace spectrum in frequency bands up to 10 MHz wide at center frequencies between 640-690 MHz. We note that these bands are just 20-30 MHz away from the frequency bands of commercial LTE deployments of the two major US cellular operators: AT&T and Verizon [11].

We use a single-antenna USRP software radio to emulate an LTE cellular phone. The USRP transmits using SC-FDMA on bandwidth up to 10 MHz on up to 1024 subcarriers, as per the LTE PHY standard [3]. Unless specified otherwise, the uplink and downlink bands are at center frequencies of 650 MHz and 680 MHz, separated by 30 MHz. We note that major US carriers separate uplink and downlink frequency bands by 30 MHz in commercial deployments.

We ensure that the characteristics of our software-radio based LTE testbed in the whitespaces closely mirror those of commercial LTE deployments. The clients transmit data only on 8% of the OFDM subcarriers, and transmit sounding reference signals once every two subframes (at most once every 2 ms, as in Verizon's LTE network configuration). In all tests we co-locate our base station with one of the LTE base stations deployed on our campus. This ensures that the multipath effects experienced by R2F2 base station closely match the multipath observed by an actual LTE deployment.

Evaluation: We perform our experiments in both indoor and outdoor settings. We co-locate our base station next to an operational LTE base stations in both settings. The client is moved to various locations across multiple buildings indoors as well as in outdoor locations along the streets and between buildings. Fig. 6 plots our testbed with the location of the base station marked in red and client locations marked as blue dots. Our experiments are performed across multiple randomly chosen client locations and the average and standard deviation of results are presented. The experiments are evenly split between outdoor and indoor locations. The experiments were conducted over three days and the weather was mostly clear, with a snow cover present throughout. Our results report both the measured signal-to-noise ratio (SNR) measured at the client as well as throughput (in Mb/s). We note that we measure throughput from SNR across LTE subcarriers using the effective SNR (ESNR) metric [17] with bit-rates adjusted based on the LTE standard [3, 50].

Note that, the delay introduced by USRP software radios (about 10 seconds) in switching frequencies limits our evaluation to static clients. While we leave an evaluation of R2-F2 for mobile clients to future work, we note that FPGA implementations of interior-point methods (like the one discussed in section 5) are fairly standard and converge in hundreds of microseconds [23]. This time is much lower than the few mili-seconds of channel coherence time for typical scenarios [48]. Finally, since R2-F2's estimates rely on uplink channels from the client to the base station, rather than the last downlink channel from the base station to the client, R2-F2's channel estimates are more recent than explicit channel feedback, thus aiding mobility.

8. Results

In this section, we present the results of an experimental evaluation of R2-F2.

8.1 Micro Benchmarks

We aim to check whether the model in §4 matches the empirical measurements. We conduct our experiments in the testbed described in §7. In each run, the base station transmits to the client, and the client computes the ground truth channels on the downlink. The client then transmits to the base station, and the base station computes the uplink channels. We run R2-F2 on the uplink channels to infer the downlink channels.

Fig. 7 plots the results from a representative run. Fig. 7(a)

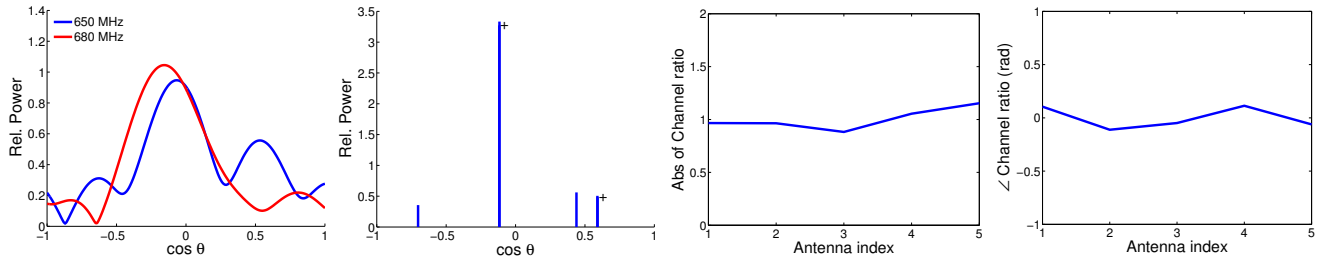

(a) (b) (c) (d)

Figure 7: **Microbenchmark:** R2-F2 measures wireless channels on the uplink at 650 MHz and predicts the downlink channels on 680 MHz. The directional power profile for the uplink channel in a particular measurement is shown in (a). We also plot the downlink profile, obtained using ground truth measurements for reference. As explained in §4, these profiles appear very different. The paths inferred by R2-F2 are plotted in (b). A '+' sign next to a path indicates presence of two paths being plotted as one due to the plotting resolution. R2-F2 uses these paths to predict channels on 680 MHz. The absolute value of the ratio of the estimated channels to the ground truth channels is plotted in (c), while (d) plots the phase of this ratio.

plots the Fourier transform of the channel measurements on uplink and downlink channels. The Fourier transform is plotted with a super resolution factor of 20, (i.e., the Fourier matrix has 5 columns that correspond to the 5 channels and 100 rows). The figure shows that the Fourier Transforms, and hence, the corresponding channels differ significantly from the downlink channels and their Fourier Transform, despite that the uplink and downlink are separated by only 30MHz. Note that, the figure shows the uplink and downlinks for the same OFDM subcarrier on each frequency band.

R2-F2 uses the measured channels on the uplink to infer the underlying physical paths. The inferred paths are shown in Fig. 7(b). The R2-F2 algorithm infers 6 different paths (two sets of two paths are clustered together due to the plotting resolution and are marked by a '+' sign in the figure). The downlink channels inferred from these paths strongly match the ground truth channels measured at the client. The ratio of the downlink channels estimated by R2-F2 and the channels measured by the client is shown in Fig. 7(c) and Fig. 7(c). Notice that the absolute value of the ratio (Fig. 7(c) is very close to 1. Moreover, the phase error in the channel ratio (Fig. 7(d) is close to zero. Thus, this example shows that the model in §4 captures the RF propagation in the testbed.

8.2 Effectiveness of Beamforming

Beamforming is the key function underlying all MIMO solutions such as MU-MIMO, massive MIMO, etc. Thus, we would like to examine whether R2-F2 can deliver the same beamforming gain as ground truth channels.

As before, we run our experiments in the testbed in Fig. 6. We repeat the experiment for different client locations, and for each client location, we collect 10 measurements. The clients were placed at distances of up to 75 meters from the base station. We measure the ground truth channels as before. We also measure the signal-to-noise ratio at the client for signals received from the base station across these experiments.

We compare the results for three different schemes: (1) Beamforming using the channels inferred by R2-F2; (2) Beamforming using the ground truth channels; and (3) Transmission in the absence of beamforming.

Fig. 8(a) depicts the CDF of the signal-to-noise ratio of these three schemes across experiments. This figure shows multiple interesting results. First, beamforming using R2-F2 provides almost the same SNR gains as beamforming using the ground truth channels. In fact, the average difference in the SNR of these two schemes is only 0.7dB. This demonstrates that R2-F2 can deliver accurate beamforming without any channel feedback, and using a completely passive channel estimation process.

Second, transmitting without beamforming reduces the SNR by an average of 6.5 dB. This result matches expectation since the theoretical gain of 5-antenna MIMO beamforming is $10\log_{10} 5 = 6.98dB$. The gains are lower at low SNR –i.e., SNR less than 3 dB. This is because channel estimation at such low SNR does not work well. This is true for both the ground truth measurement at the client and the uplink measurements at the base station.

In order to evaluate the throughput improvement, we plot the data rates associated with the SNRs for all three schemes in Fig. 8(b). The figure shows that R2-F2 can double or tripple throughput in our testbed. The average throughput increase is 1.7x. The throughput gains are large at low to moderate SNRs but are less at higher SNR. This is expected since the rate is the log of the SNR. Also, at SNR more than 20dB, the highest data rate is achieved and beamforming doesn't help in increasing the rate. Similar to Fig. 8(a), the beamforming gains are low at SNR less than 3 dB. This is because at such low SNR, channel measurements become noisy, giving R2-F2 a noisy input.

8.3 Performance as a Function of Channel Separation

We study R2-F2's performance as a function of the separation between the uplink and downlink channels. We repeat our experiments by changing the separation between uplink and downlink frequency bands between 10 MHz and 40 MHz within the whitespace band of frequencies. Limitations of our white space license do not let us go beyond the 40 MHz separation. We measure R2-F2's SNR gain due to beamforming, for users at different randomly chosen locations in the testbed. Fig. 8(c) plots the mean and standard deviation of gain in SNR using R2-F2's beamforming, across different separations of uplink and downlink frequency bands. As expected, R2-F2's gain improves

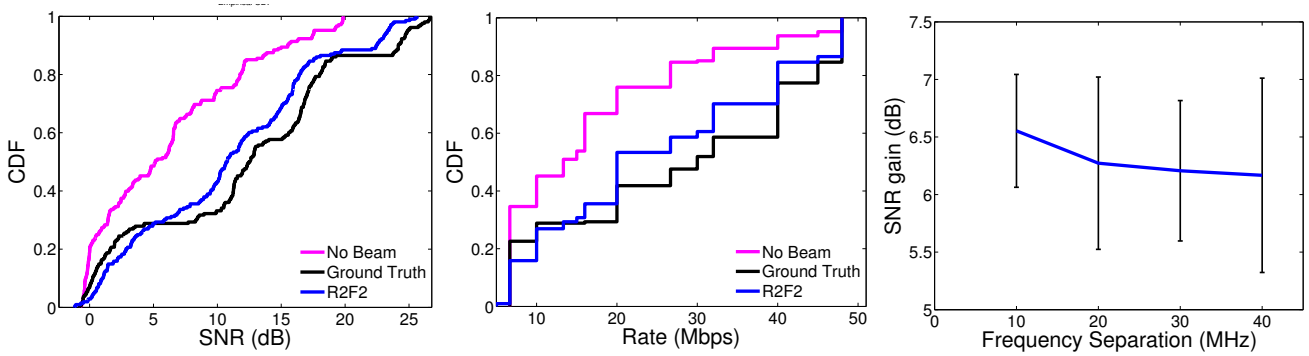

(a) (b) (c)

Figure 8: **Beamforming:** We use the channels estimated by R2-F2 to achieve beamforming towards the client. Figure (a) depicts the CDF of the SNR at the client without beamforming, using beamforming with the channels predicted by R2-F2 and using beamforming with the true channels measured at the client. R2-F2 achieves ~6 dB SNR gain over no beamforming, which is just 0.7 dB less than beamforming with ideal channels. Figure (b) depicts the datarates achieved by the different schemes. R2-F2 enables a median gain of 1.7x in datarate for clients in our testbed. Figure (c) depicts the median gain in SNR due to beamforming using channels estimated by R2-F2 as a function of frequency separation.

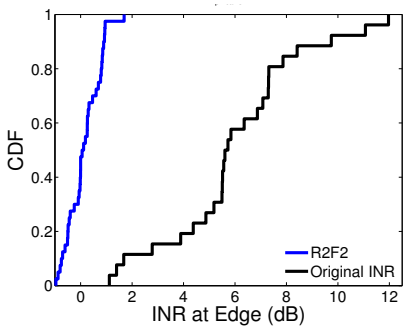

Figure 9: **Nulling interference at Edge Clients:** R2-F2 can reduce inter-cell interference by enabling the base station to null it's signal to the clients at the cell edge. R2-F2 reduces the interference at the edge from a median of 5.5 dB to 0.2 dB and the 90th percentile from 9 dB to 0.9 dB.

with a lower separation, with the highest gain achieved for a 10 MHz separation (6.55 dB). However, we observe that the SNR reduced very slowly with increase in downlink-uplink separation. Since the separation between the LTE downlink and uplink for most of the Verizon and AT&T deployments are 20MHz and 30MHz respectively, we believe that R2-F2 can be used to eliminate channel feedback in these networks. A potential cause of the degradation of the performance of R2-F2 with larger frequency separations is the variation in reflection properties of materials across frequencies, as observed in [35] in the context of GPS signals.

8.4 Interference Nulling at Edge Clients

Clients at cell edge can suffer a significant amount of interference from neighboring cells which could amount to 10 to 12dB [46]. R2-F2 can be used to reduce interference at edge-clients located at cell boundaries using interference nulling. To evaluate this function, we set up our base station as in Fig. 6, but we move the client to the edge of the cell to emulate a client from a neighboring cell. We repeat the experiment from the previous section. However instead of using the inferred downlink channels to beamform, the base station uses the channels to perform interference nulling.

Fig. 9 plots a CDF of the interference power before and after nulling. The figure shows that R2-F2 dramatically reduces the interference at edge clients. In particular, the average INR (interference to noise ratio) is reduced from 5.5 dB to 0.2 dB, and the 90th percentile from 9 dB to 0.9 dB. This shows that R2-F2 can be used beyond coherent beamforming, to counter inter-cell interference.

8.5 Comparison with Angle-of-Arrival Power Profile

At this stage, one might wonder if it is possible to achieve gains similar to R2-F2 by using the angle-of-arrival (AoA) power profiles similar to the ones shown in Fig. 2 and Fig. 3(d). In principle, one could use the measured wireless channels on one frequency to compute the AoA power profile using standard AoA equations. Then, this angle-of-arrival profile can be treated as a signature of the underlying physical propagation and can be used to compute the channels at the target frequency band. We conduct experiments on our testbed to evaluate this approach and compare the gains achieved by R2-F2 with the gains achieved by the AoA profile.

Beamforming: We compare the beamforming gain achieved by R2-F2 with the gains achieved with the AoA-based approach. The CDF of the signal to noise ratios achieved with the two approaches is compared in Fig. 10(a). While the AoA approach increases the median SNR of the testbed by 2.8 dB, the gain is much lower than R2-F2 which increases the SNR of the testbed by 6.3 dB. This is understandable, given the intuition developed in section 4 and 5. While the AoA power profiles of the signal have the same underlying paths, they are inherently dependent on frequency. Thus, using these profiles directly to estimate channels across frequencies leads to errors in the estimation.

Nulling at Edge Clients: Similar to §8.4, we aim to null the interference caused by the base station at the edge clients. We use the channels estimated using the AoA approach to null the interfering signal at the client. The CDF of the INR (in-

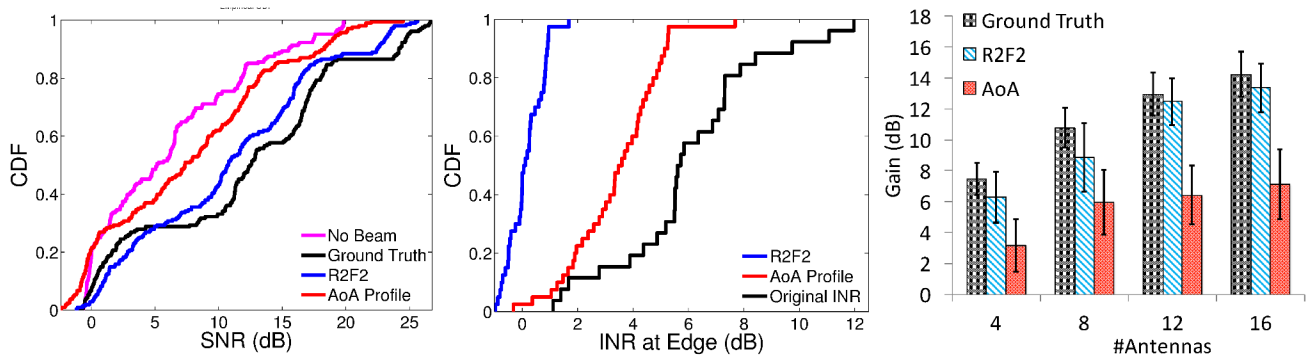

(a) (b) (c)

Figure 10: **Comparison with AoA Power Profile:** (a) AoA profile based channel estimation increases the median SNR of the testbed by 2.8 dB (as opposed to 6.3 dB for R2-F2). (b) Interference at the edge clients can be brought down from a median of 5.5 dB to 3.5 dB. However, R2-F2 outperforms this approach by nulling to 0.2 dB (median). (c) Simulation results show that with increase in number of antennas, the gain achieved by R2-F2 closely follows the ideal beamforming gain.

terference to noise ratio) after nulling is shown in Fig. 10(b). The median interference SNR is reduced from 5.5 dB to 3.5 dB. However, as expected, the errors in channel estimates prevent it from going down to the median SNR achieved by R2-F2 (0.2 dB).

Variation with Number of Antennas: Finally, it is natural to ask if, with the increase in the number of antennas, the sinc functions plotted in Fig. 3 (c), start to become narrower and thus, two sincs for different paths do not impact each other. This would lead to the AoA power profiles in Fig. 3 (d) to look identical at different frequencies and hence, improve the performance of this approach.

Since we have a 5 antenna base station, we are unable to test this hypothesis empirically. However, we test this hypothesis using a simulation. We simulate a wireless testbed of size 200 $m \times 200$ m. Channels are modeled using equation the standard wireless propagation model (Eqn. 2 [47]). The signals from the base station to the client and vice-versa travel through the direct line of sight path and also after reflecting off up to 10 different obstacles along the way. The positions of the reflectors are randomly selected and so is the attenuation faced by each path. The number of antennas on the base station is varied from 4 to 16 in steps of 4. The frequency of operation is 650 MHz (uplink) and 680 MHz (downlink), as used in the rest of the results. Random additive white Gaussian noise is added in order to vary the SNR.

We plot the variation of the SNR gains achieved by different systems in Fig. 10(c). As the number of antennas increases, the ideal beamforming gain with the true channels increases as $20log(N)$ on average, where N is the number of antennas. R2-F2 keeps up with this increase in gain, as the number of antennas increases and stays within 1 dB of the ideal gain. With more antennas, R2-F2 has more information to estimate the path parameters underlying the wireless channels and hence, improves its estimates. On the other hand, the AoA profile based approach can only achieve half of the gain achieved by the beamforming with the true channel information, even as the number of antennas is increased to 16. This is because of two main reasons: a) as the number of antennas increases, the directionality of the antenna array increases and hence, a better estimation of channels is required to maintain the ideal gain and b) even if the sincs become narrower, as is expected, with increasing number of antennas, the phase of each of the sincs is still frequency dependent. When these sincs combine to give the channels, these phase add errors in the channel estimates.

To conclude, this simulation provides two interesting insights. First, R2-F2 maintains its performance even as the number of antennas is increased. Second, it does not suffice to use AoA power profiles to infer wireless channels at the target frequency. One needs to go further and separate the individual paths and their phases to achieve accurate channel inference, as done by R2-F2.

9. Concluding Remarks

In this paper, we present, R2-F2 a system that uses wireless channel measurements on one frequency band to infer channels on a different frequency band. By doing so, R2-F2 enables multi-antenna techniques to be used in LTE systems with *zero* feedback from the client. R2-F2's performance was demonstrated empiricaly with uplink and downlink channels separated by 20-30 MHz, as in the majority of LTE deployments in United States [49]. Beyond LTE, our work has implications on the general concept of reciprocity across frequency bands, for other wireless technologies such as wireless LANs and whitespace networks. However, we note that the relatively small separation of uplink and downlink frequencies in LTE ensures that reflection properties of objects in the environment and the divergence between physical propagation characteristics is limited. We believe extending the results presented by us to technologies that require significantly larger frequency separations is non-trivial and falls in the realm of future work.

Acknowledgements: We thank the NETMIT group, Arthur Berger, our reviewers and our shepherd, Deepak Ganesan, for their insightful comments. This work is funded by MIT Lincoln Laboratory. We thank members of the MIT Center for Wireless Networks and Mobile Computing: Amazon, Cisco, Google, Intel, Mediatek, Microsoft, ST Microelectronics and Telefonica for their interest and support.

10. REFERENCES

[1] 3rd Generation Partnership Project. Evolved Universal Terrestrial Radio Access (E-UTRA), Physical Layer Procedures (Release 8), 3GPP TS 36.213, v8.8.0. Oct 2009.

[2] 3rd Generation Partnership Project. Evolved Universal Terrestrial Radio Access (E-UTRA), Multiplexing and Channel Coding (Release 8), 3GPP TS 36.212, v8.8.0. Jan 2010.

[3] 3rd Generation Partnership Project. Evolved Universal Terrestrial Radio Access (E-UTRA), Physical Channels and Modulation (Release 8), 3GPP TS 36.211, v8.9.0. Jan 2010.

[4] O. Abari, D. Vasisht, D. Katabi, and A. Chandrakasan. Caraoke: An e-toll transponder network for smart cities. In *ACM SIGCOMM*, 2015.

[5] I. F. Akyildiz, D. M. Gutierrez-Estevez, and E. C. Reyes. The evolution to 4g cellular systems: Lte-advanced. *Physical Communication*, 3(4):217–244, 2010.

[6] W. U. Bajwa, J. Haupt, A. M. Sayeed, and R. Nowak. Compressed channel sensing: A new approach to estimating sparse multipath channels. *Proceedings of the IEEE*, 98(6):1058–1076, 2010.

[7] A. Canavitsas, L. Mello, and M. Grivet. White space prediction technique for cognitive radio applications. In *Microwave Optoelectronics Conference (IMOC), 2013 SBMO/IEEE MTT-S International*, pages 1–5, Aug 2013.

[8] W. Cao and W. Wang. A frequency-domain channel prediction algorithm in wideband wireless communication systems. In *Personal, Indoor and Mobile Radio Communications, 2004. PIMRC 2004. 15th IEEE International Symposium on*, volume 4, pages 2402–2405 Vol.4, Sept 2004.

[9] J. Choi, D. J. Love, and P. Bidigare. Downlink training techniques for fdd massive mimo systems: Open-loop and closed-loop training with memory. *Selected Topics in Signal Processing, IEEE Journal of*, 8(5):802–814, 2014.

[10] R. Crepaldi, J. Lee, R. Etkin, S.-J. Lee, and R. Kravets. Csi-sf: Estimating wireless channel state using csi sampling amp; fusion. In *INFOCOM, 2012 Proceedings IEEE*, pages 154–162, March 2012.

[11] P. Denisowski. Recognizing and resolving lte/catv interference issues. *White Paper, Rohde and Schwarz*, 2011.

[12] L. Dong, G. Xu, and H. Ling. Prediction of fast fading mobile radio channels in wideband communication systems. In *Global Telecommunications Conference, 2001. GLOBECOM'01. IEEE*, volume 6, pages 3287–3291. IEEE, 2001.

[13] A. ElNashar, M. El-saidny, and M. Sherif. *Design, Deployment and Performance of 4G-LTE Networks: A Practical Approach*. John Wiley & Sons, 2014.

[14] R. Ghaffar and R. Knopp. Interference-aware receiver structure for multi-user mimo and lte. *EURASIP Journal on Wireless Communications and Networking*, 2011(1):1–17, 2011.

[15] S. Gollakota, S. Perli, and D. Katabi. Interference alignment and cancellation. *SIGCOMM*, 2009.

[16] M. Guillaud, D. Slock, and R. Knopp. A practical method for wireless channel reciprocity exploitation through relative calibration. *ISSPA*, 2005.

[17] D. Halperin, W. Hu, A. Sheth, and D. Wetherall. Predictable 802.11 packet delivery from wireless channel measurements. *ACM SIGCOMM Computer Communication Review*, 41(4):159–170, 2011.

[18] Y. Han, J. Ni, and G. Du. The potential approaches to achieve channel reciprocity in fdd system with frequency correction algorithms. In *Communications and Networking in China (CHINACOM), 2010 5th International ICST Conference on*, pages 1–5, Aug 2010.

[19] K. Hugl, K. Kalliola, and J. Laurila. Spatial reciprocity of uplink and downlink radio channels in fdd systems. 2002.

[20] S. Imtiaz, G. S. Dahman, F. Rusek, and F. Tufvesson. On the directional reciprocity of uplink and downlink channels in frequency division duplex systems. In *IEEE Symposium on Personal Indoor and Mobile Radio Communications*, 2014.

[21] T. Innovations. Lte in a nutshell. *White paper*, 2010. https://home.zhaw.ch/kunr/NTM1/literatur/LTE%20in%20a%20Nutshell%20-%20Physical%20Layer.pdf.

[22] R. Irmer, H. Droste, P. Marsch, M. Grieger, G. Fettweis, S. Brueck, H.-P. Mayer, L. Thiele, and V. Jungnickel. Coordinated multipoint: Concepts, performance, and field trial results. *Communications Magazine, IEEE*, 49(2):102–111, 2011.

[23] J. L. Jerez, G. A. Constantinides, and E. C. Kerrigan. Fpga implementation of an interior point solver for linear model predictive control. In *Field-Programmable Technology (FPT), 2010 International Conference on*, pages 316–319, Dec 2010.

[24] H. Ji, Y. Kim, J. Lee, E. Onggosanusi, Y. Nam, J. Zhang, B. Lee, and B. Shim. Overview of full-dimension mimo in lte-advanced pro. *arXiv preprint arXiv:1601.00019*, 2015.

[25] F. Kaltenberger, D. Gesbert, R. Knopp, and M. Kountouris. Performance of multi-user mimo precoding with limited feedback over measured channels. In *Global Telecommunications Conference, 2008. IEEE GLOBECOM 2008. IEEE*, pages 1–5. IEEE, 2008.

[26] F. Kaltenberger, H. Jiang, M. Guillaud, and R. Knopp. Relative channel reciprocity calibration in mimo/tdd systems. In *Future Network and Mobile Summit, 2010*, pages 1–10. IEEE, 2010.

[27] M. Kotaru, K. Joshi, D. Bharadia, and S. Katti. Spotfi: Decimeter level localization using wifi. In *Proceedings of the 2015 ACM Conference on Special Interest Group on Data Communication*, SIGCOMM '15, 2015.

[28] S. Kumar, S. Gil, D. Katabi, and D. Rus. Accurate indoor localization with zero start-up cost. MobiCom, 2014.

[29] S. Kumar, E. Hamed, D. Katabi, and L. E. Li. LTE Radio Analytics Made Easy and Accessible. SIGCOMM, 2014.

[30] T. Kwon, Y.-G. Lim, and C.-B. Chae. Limited channel feedback for rf lens antenna based massive mimo systems. In *Computing, Networking and Communications (ICNC), 2015 International Conference on*, pages 6–10. IEEE, 2015.

[31] E. Larsson, O. Edfors, F. Tufvesson, and T. Marzetta. Massive mimo for next generation wireless systems. *Communications Magazine, IEEE*, 52(2):186–195, 2014.

[32] D. Lee, H. Seo, B. Clerckx, E. Hardouin, D. Mazzarese, S. Nagata, and K. Sayana. Coordinated multipoint transmission and reception in lte-advanced: deployment scenarios and operational challenges. *Communications Magazine, IEEE*, 50(2):148–155, 2012.

[33] K. C.-J. Lin, S. Gollakota, and D. Katabi. Random access heterogeneous mimo networks. *ACM SIGCOMM Computer Communication Review*, 41(4):146–157, 2011.

[34] Y.-H. Nam, M. S. Rahman, Y. Li, G. Xu, E. Onggosanusi, J. Zhang, and J.-Y. Seol. Full dimension mimo for lte-advanced and 5g. *IEEE Communications Magazine*, 2013.

[35] S. Nirjon, J. Liu, G. DeJean, B. Priyantha, Y. Jin, and T. Hart. Coin-gps: Indoor localization from direct gps receiving. In *Proceedings of the 12th Annual International Conference on Mobile Systems, Applications, and Services*, MobiSys '14, pages 301–314, New York, NY, USA, 2014. ACM.

[36] N. Palleit and T. Weber. Obtaining transmitter side channel state information in mimo fdd systems. In *Personal, Indoor and Mobile Radio Communications, 2009 IEEE 20th International Symposium on*, pages 2439–2443. IEEE, 2009.

[37] N. Palleit and T. Weber. Channel prediction in point-to-point mimo-systems. In *Wireless Communication Systems (ISWCS), 2010 7th International Symposium on*, pages 91–95. IEEE, 2010.

[38] B. Radunovic, A. Proutiere, D. Gunawardena, and P. Key. Dynamic channel, rate selection and scheduling for white spaces. In *Proceedings of the Seventh COnference on emerging Networking EXperiments and Technologies*, page 2. ACM, 2011.

[39] H. Rahul, S. Kumar, and D. Katabi. MegaMIMO: Scaling Wireless Capacity with User Demands. In *ACM SIGCOMM 2012*, Helsinki, Finland, August 2012.

[40] X. Rao and V. K. N. Lau. Distributed compressive CSIT estimation and feedback for FDD multi-user massive MIMO systems. *CoRR*, abs/1405.2786, 2014.

[41] M. Roetter. Spectrum for mobile broadband in the americas: Policy issues for growth and competition. 2011.

[42] S. Sen, B. Radunovic, J. Lee, and K.-H. Kim. Cspy: Finding the best quality channel without probing. In *Proceedings of the 19th annual international conference on Mobile computing & networking*, pages 267–278. ACM, 2013.

[43] L. Shi, P. Bahl, and D. Katabi. Beyond sensing: Multi-ghz realtime spectrum analytics. In *12th USENIX Symposium on Networked Systems Design and Implementation (NSDI 15)*, pages 159–172, Oakland, CA, May 2015. USENIX Association.

[44] T. Shuang, T. Koivisto, H.-L. Maattanen, K. Pietikainen, T. Roman, and M. Enescu. Design and evaluation of lte-advanced double codebook. In *Vehicular Technology Conference (VTC Spring), 2011 IEEE 73rd*, pages 1–5, May 2011.

[45] M. S. Sim and C.-B. Chae. Compressed channel feedback for correlateci massive mimo systems. In *Globecom Workshops (GC Wkshps), 2014*, pages 327–332. IEEE, 2014.

[46] S. Sun, Q. Gao, Y. Peng, Y. Wang, and L. Song. Interference management through comp in 3gpp lte-advanced networks. *Wireless Communications, IEEE*, 20(1):59–66, 2013.

[47] D. Tse and P. Vishwanath. *Fundamentals of Wireless Communications*. Cambridge University Press, 2005.

[48] D. Tse and P. Vishwanath. *Fundamentals of Wireless Communications*. Cambridge University Press, 2005.

[49] H. Victor. Which 4G LTE bands do ATT, Verizon, T-Mobile and Sprint use in the USA? http://www.phonearena.com/news/Cheat-sheet-which-4G-LTE-bands-do-AT-T-Verizon-T-Mobile-and-Sprint-use-in-the-USA_id77933.

[50] O. Werther and R. Minihold. Lte system specifications and their impact on rf & base band circuits. *Application Note, Rohde and Schwarz*, 2013.

[51] I. C. Wong and B. L. Eva. Joint channel estimation and prediction for ofdm systems. In *Global Telecommunications Conference, 2005. GLOBECOM'05. IEEE*, volume 4, pages 5–pp. IEEE, 2005.

[52] L. Wu, J. Chen, H. Yang, and D. Lu. Codebook design for lte-a downlink system. In *Vehicular Technology Conference (VTC Fall), 2011 IEEE*, pages 1–5, Sept 2011.

[53] J. Xiong and K. Jamieson. Arraytrack: A fine-grained indoor location system. NSDI '13, 2013.

[54] Y. Xu, G. Yue, and S. Mao. User grouping for massive mimo in fdd systems: New design methods and analysis. *Access, IEEE*, 2:947–959, 2014.

[55] T. Zhang, N. Leng, and S. Banerjee. A vehicle-based measurement framework for enhancing whitespace spectrum databases. In *Proceedings of the 20th Annual International Conference on Mobile Computing and Networking*, MobiCom '14, pages 17–28, New York, NY, USA, 2014. ACM.